ANTIOXIDANTS & REDOX SIGNALING
Volume 14, Number 12, 2011

DOI: 10.1089/ars.2010.3399



# Dissection of the Xeroderma Pigmentosum Group C Protein Function by Site-Directed Mutagenesis

Flurina C. Clement,[1] Nina Kaczmarek,[1] Nadine Mathieu,[1] Martin Tomas,[2] Alfred Leitenstorfer,[2] Elisa Ferrando-May,[3] and Hanspeter Naegeli[1]

## Abstract

Xeroderma pigmentosum group C (XPC) protein is a sensor of helix-distorting DNA lesions, the function of which is to trigger the global genome repair (GGR) pathway. Previous studies demonstrated that XPC protein operates by detecting the single-stranded character of non–hydrogen-bonded bases opposing lesion sites. This mode of action is supported by structural analyses of the yeast Rad4 homologue that identified critical side chains making close contacts with a pair of extrahelical nucleotides. Here, alanine substitutions of the respective conserved residues (N754, F756, F797, F799) in human XPC were tested for DNA-binding activity, accumulation in tracks and foci of DNA lesions, nuclear protein mobility, and the induction of downstream GGR reactions. This study discloses a dynamic interplay between XPC protein and DNA, whereby the association with one displaced nucleotide in the undamaged strand mediates the initial encounter with lesion sites. The additional flipping-out of an adjacent nucleotide is necessary to hand over the damaged site to the next GGR player. Surprisingly, this mutagenesis analysis also reveals that the rapid intranuclear trafficking of XPC protein depends on constitutive interactions with native DNA, implying that the search for base damage takes place in living cells by a facilitated diffusion process. *Antioxid. Redox Signal.* 14, 2479–2490.

## Introduction

Nucleotide excision repair is a fundamental cytoprotective system that removes bulky DNA adducts and intrastrand crosslinks generated by ultraviolet (UV) light, genotoxic chemicals, reactive metabolic intermediates, and oxygen radicals, as well as lipid peroxidation products (18, 19, 21, 35, 46). Two distinct subpathways of this versatile DNA-repair process have been discerned, depending on the genomic context. Transcription-coupled repair eliminates DNA lesions from the transcribed strand of active genes, whereas global-genome repair (GGR) excises base damage from any sequence including nontranscribed strands and silent domains (17, 20). The relevance of an effective DNA-repair surveillance is highlighted by the inherited disorder xeroderma pigmentosum (XP), in which defects in the GGR pathway lead to a >1,000-fold increased incidence of sunlight-induced skin cancer. XP patients also have a higher risk of developing internal tumors and often have neurologic deterioration or other traits of premature aging attributable to oxidative stress (2, 6, 11). The disease can be classified into seven repair-deficient complementation groups, designated XP-A through XP-G (12, 27).

XPC protein is the 940-amino-acid DNA-binding constituent of a promiscuous sensor that associates with damaged sites to initiate the GGR reaction (4, 39, 44). The other two subunits of this initiator complex, Rad23B and centrin-2, have an accessory function in stabilizing XPC and stimulating its recognition function (31, 32). XPC protein provides a landing platform for transcription factor TFIIH (48), whose unwinding activity, assisted by XPA and replication protein A (RPA), generates an open nucleoprotein intermediate in which the DNA is melted over 25 to 30 nucleotides (15, 45). The double- to single-stranded transitions at the borders of this open complex are cleaved by structure-specific endonucleases, thereby releasing the offending lesion by dual DNA incision (23, 33, 36). Finally, repair-patch synthesis is carried out by the coordinated activity of DNA polymerases and ligases (3, 37).

Against the conventional dogma that DNA lesions are recognized through direct contacts with modified nucleotides, XPC protein distinguishes between damaged DNA and the native double helix by sensing the single-stranded character of non–hydrogen-bonded bases in the undamaged strand (7, 28, 42). This view was confirmed when a crystallographic analysis of the yeast Rad4 homologue revealed the bimodal binding scheme of this versatile factor (30). One part

[1]Institute of Pharmacology and Toxicology, University of Zürich-Vetsuisse, Zürich, Switzerland.
[2]Department of Physics and Center for Applied Photonics, University of Konstanz, Konstanz, Germany.
[3]Bioimaging Center, University of Konstanz, Konstanz, Germany.

of Rad4 protein, involving its large transglutaminase homology domain and a short $\beta$-hairpin domain (BHD1), associates with 11 base pairs of duplex DNA flanking the lesion. A second part, comprising $\beta$-hairpin domains BHD2 and BHD3, interacts with a four-nucleotide segment of the undamaged strand opposing the lesion. Two of these undamaged nucleotides are displaced out of the double helix and accommodated into a handlike Rad4 protein fold, where the DNA adopts the configuration of a single-stranded overhang (38). The amino acids making contacts with these extrahelical nucleotides are evolutionarily conserved (Fig. 1A) and, therefore, it can be predicted from the Rad4 structure that N754 and F756 of human XPC interact with one flipped-out base, located on the 3′ side, whereas F799 binds to the second flipped-out nucleotide on the 5′ side, and F797 interacts with both extrahelical residues simultaneously (Fig. 1B).

The presence of two fully extruded nucleotides in the Rad4–DNA complex is intriguing because most helix-distorting lesions, including those that are readily excised by the GGR system, cause the destabilization of just a single base pair. For example, UV light–induced (6-4) photoproducts interfere with the Watson–Crick hydrogen-bonding pattern of only one modified pyrimidine, whereas all surrounding base pairs retain their native double helical geometry (24, 25). Similarly, the rapidly excised (+)-*cis*-benzo[*a*]pyrene-$N^2$-dG or *N*-acetyl-2-aminofluorene-dG adducts disrupt only the Watson–Crick pairing between the modified guanines and their cytosine partners (13, 34). This discrepancy between the limited base-pair destabilization induced by many GGR substrates and the more extensive base displacement in the Rad4 co-crystal raises the twofold questions of how this factor and its human counterpart are able to find lesions embedded in native genomic DNA and what is the function of the extensive conformational changes observed in the Rad4 crystal complex.

To address these unresolved issues, residues N754, F756, F797, and F799 of the human XPC sequence, which are predicted to accommodate the two flipped-out nucleotides in their outward position, were subjected to site-directed mutagenesis. The biochemical properties of the resulting alanine mutants were tested both *in vitro* and in living cells to determine the contribution of each individual side chain to the molecular search process, the detection of lesions, and formation of a stable recognition intermediate, as well as the induction of downstream reactions. This report provides new insights into dynamic aspects of the genome-wide search mechanism by which XPC protein finds DNA damage and initiates the versatile GGR pathway.

## Materials and Methods

### *XPC constructs and mutants*

The human *XPC* complementary DNA was cloned into pEGFP-N3 (Clontech, Mountain View, CA) by using the restriction enzymes *Xma*I and *Kpn*I and into the pFastBac HTc vector (Invitrogen, Basel, Switzerland) with *Not*I and *Kpn*I. Mutations were generated by site-directed mutagenesis (QuickChange; Stratagene, Heidelberg, Germany) by using the primers 5′-gaaggtgccccgggccgagtttgggaatgtgtac-3′ (N754A), 5′-gaaggtgccccggaacgaggctgggaatgtgtac-3′ (F756A),

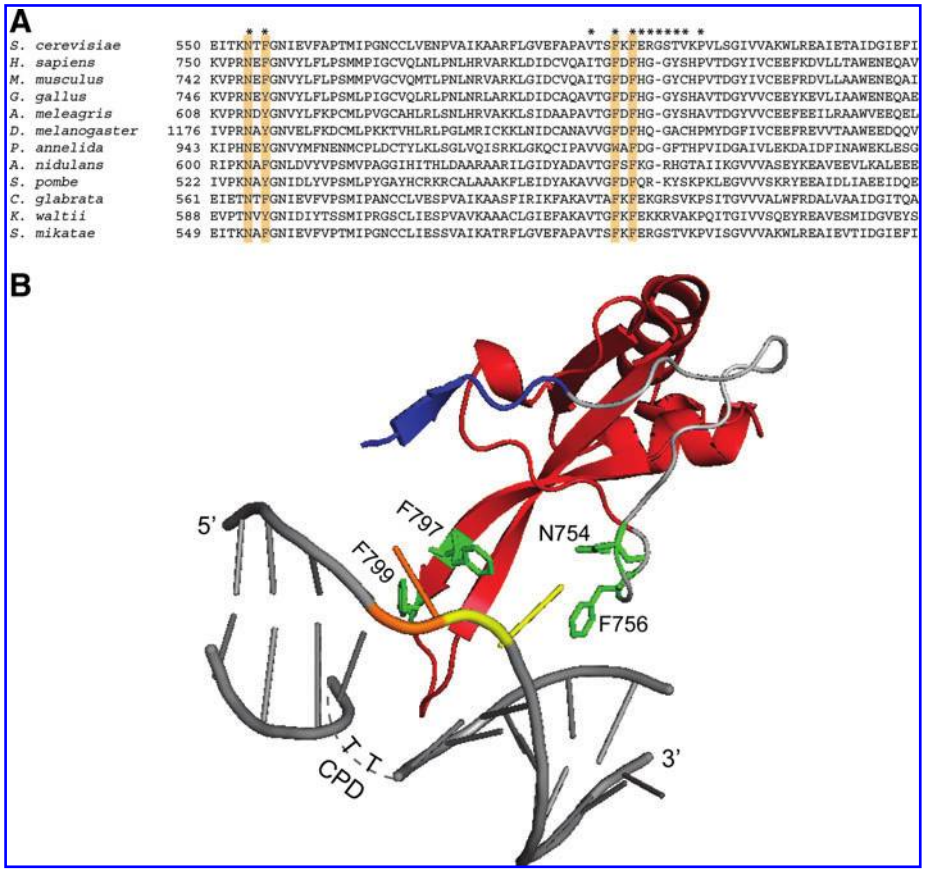


**FIG. 1. Conserved amino acids interacting with flipped-out nucleotides. (A)** Sequence comparison centered on the protein domain of eukaryotic XPC homologues (residues 750–833 of the human polypeptide) predicted to interact with flipped-out nucleotides. The asterisks denote amino acid side chains of Rad4 protein that interact directly with DNA (30). The residues targeted for site-directed mutagenesis are indicated in orange. **(B)** Ribbon diagram of the predicted XPC domain that associates with two flipped-out nucleotides. N754 and F756 interact with the displaced nucleotide on the 3′ side, F799 with the displaced nucleotide on the 5′ side, and F797 interacts with both residues simultaneously. CPD, cyclobutane pyrimidine dimer. The figure was made with the PyMol Molecular Viewer by using the coordinates PDB 2QSG. (To see this illustration in color the reader is referred to the web version of this article at www.liebertonline.com/ars).

5′-caggccatcactggcgctgatttccatggcggc-3′ (F797A), and 5′-ccatc actggctttgatgcccatggcggctactcc-3′ (F799A) from Microsynth (Balgach, Switzerland). All resulting clones were sequenced to exclude concomitant accidental mutations.

### *XPC expression in insect cells*

The vector pFastBac HTc containing the human *XPC* sequence, fused to $His_6$ and maltose-binding protein (MBP) tags (28), was introduced into recombinant baculovirus by using the BAC-TO-BAC Baculovirus Expression System (Invitrogen). *Sf*9 cells ($2\times10^6$) were infected, and cell lysates containing $His_6$-MBP-XPC fusion proteins were obtained as described (43). Each *Sf*9 cell lysate was analyzed by denaturing polyacrylamide gel electrophoresis, Coomassie staining, and immunoblotting with antibodies against $His_6$ (Sigma, Buchs, Switzerland). The amount of human XPC protein was determined by comparing the intensity of the $His_6$-MBP-XPC band of ~170 kDa with that of a bovine serum albumin standard (Fluka, Basel, Switzerland).

### *DNA-binding assay*

Double-stranded and junction DNA probes were produced by hybridization of a $^{32}$P-labeled 135-mer with fully or partially complementary 135-mers (Microsynth) in 50 m*M* Tris–HCl (pH 7.4), 10 m*M* $MgCl_2$, and 1 m*M* dithiothreitol (DTT). Complete hybridization of the radiolabeled strand was demonstrated by analysis of the duplex and junction DNA products on native 5% (wt/vol) polyacrylamide gels. The indicated concentrations of XPC protein, as part of *Sf*9 cell lysates (5–25 $\mu$l), were incubated with $^{32}$P-labeled 135-mer substrates (2 n*M*) in 200 $\mu$l buffer A [25 m*M* Tris–HCl, pH 7.5, 0.3 *M* NaCl, 10% (vol/vol) glycerol, 0.01% (vol/vol) Triton X-100, 0.25 m*M* phenylmethane sulfonyl fluoride, and 1 m*M* EDTA). After 1.5 h at 4°C, the reaction mixtures were supplemented with monoclonal antibodies against MBP linked to paramagnetic beads (0.2 mg; New England BioLabs, Bioconcept, Allschwil, Switzerland). After another 1 h at 4°C, the beads were washed twice with 200 $\mu$l buffer A, and the radioactivity associated with the paramagnetic beads was quantified with liquid scintillation counting. All values were corrected for the background resulting from control incubations with a lysate from uninfected cells.

### *Cell culture*

All cell-culture media and supplements were from Invitrogen. Simian virus 40–transformed human XP-C fibroblasts (GM16093), derived from patient XP14BR, were obtained from the Coriell Institute for Medical Research (Camden, NJ). These cells carry a homozygous C-to-T transition at codon 718, leading to a nonfunctional truncate (10). The XP-C fibroblasts were grown in a humidified incubator at 37°C and 5% $CO_2$ by using Dulbecco's modified Eagle's medium (DMEM) supplemented with 10% heat-inactivated fetal calf serum (FCS), 100 units/ml penicillin G, and 100 $\mu$g/ml streptomycin. Chinese hamster ovary (CHO) cells were cultured as were the XP-C fibroblasts, except that DMEM was replaced by F-12 Nutrient Mixture.

### *Transfections*

The 500,000 XP-C or 250,000 CHO cells were seeded into six-well plates. After 24 h, at a confluence of 80–85%, the cells were transfected with 1 $\mu$g XPC-pEGFP-N3 or pEGFP-DDB2-C1 plasmids by using 4 $\mu$l FuGENE HD transfection reagent (Roche, Basel, Switzerland). After a 4-h incubation, the transfection mixture was replaced by complete culture medium, and the cells were incubated for another 18 h at 37°C. The expression of XPC-GFP constructs was assessed with immunoblotting by using monoclonal antibodies against human XPC protein (Abcam, Cambridge, England).

### *High-resolution DNA-damage induction*

Multiphoton laser irradiation is a powerful tool to induce narrow areas of DNA damage in the nuclei of mammalian cells (29). CHO cells were grown in a $\mu$-Dish, 35 mm high (Ibidi, München, Germany), and, 18 h after transfection, the medium was replaced by phenol red–free DMEM supplemented with 10% FCS and 25 m*M* HEPES (pH 7.2). Single nuclei were irradiated along a 10-$\mu$m track with a multiphoton fiber laser coupled to a confocal microscope (LSM Pascal, Zeiss, Göttingen, Germany). The laser generates pulses of 775 nm with a duration of 290 femtoseconds and a repetition rate of 107 MHz (41). By multiphoton excitation, three colliding photons of low energy (775 nm wavelength) cause DNA lesions that would normally arise from the absorption of a single photon at higher energy (258 nm wavelength). The peak power density at the focal plane was 365 GW/cm$^2$, and the pixel dwell time was 44.2 ms, generating approximately 5,000 UV lesions [cyclobutane pyrimidine dimers and (6-4) photoproducts] in each treated cell (8). The area of each irradiation track was $<10\ \mu m^2$, and its volume, $<20\ \mu m^3$.

### *Induction of UV foci*

CHO cells were grown on glass coverslips (20 mm diameter) and transfected with XPC-GPF constructs, as described. After 18-h incubations, the cell-culture medium was removed, and the cells were rinsed with phosphate-buffered saline (PBS). UV foci were induced by irradiation through the 5-$\mu$m pores of polycarbonate filters (Millipore, Zug, Switzerland) by using a UV-C source (254 nm, 150 J/m$^2$). Immediately after irradiation, the filters were gently removed, and the cells incubated for the indicated periods at 37°C in complete DMEM.

### *Immunocytochemistry*

All procedures were performed at room temperature, unless otherwise stated. At the indicated times after irradiation, cells were washed and fixed for 15 min by using 4% (wt/vol) paraformaldehyde in PBS. The cells were permeabilized with PBS containing 0.1% (vol/vol) TWEEN 20 for 10 min, and DNA was denatured with 0.07 *M* NaOH for 8 min. Subsequently, the samples were washed 5 times with 0.1% TWEEN 20 and blocked (30 min at 37°C) with 20% FCS in PBS. The samples were incubated (1 h at 37°C in PBS containing 5% FCS) with primary antibodies directed against (6-4) photoproducts (MBL International Corporation, Woburn, MA) (dilution,1:1,000) or against the p62 (Abcam) and p89 subunits of TFIIH (Santa Cruz Biotechnology, Santa Cruz, CA) (dilution, 1:250). Next, the samples were washed with 0.1% TWEEN 20, blocked twice for 10 min with 20% FCS, and incubated with Alexa Fluor 594-conjugated secondary antibodies (Invitrogen) (dilution, 1:400) for 30 min at 37°C. After washing with 0.1% TWEEN 20 in PBS, the nuclei were stained

for 10 min with Hoechst dye 33258 (200 ng/ml). Finally, the samples were washed 3 times with PBS and analyzed by using an oil-immersion objective.

### *Image analysis*

Fluorescence measurements in UV tracks were carried out through a ×40 oil-immersion objective lens with a numeric aperture of 1.4 (EC-Plan-Neo-Fluar, Zeiss) by using an $Ar^+$ source (488 nm wavelength). The selected parameters (laser power and magnification factor) were kept constant throughout all experiments. For real-time recordings, an image was taken every 5 s for up to 105 s after irradiation and analyzed with the ImageJ software (http://rsb.info.nih.gov/ij), including corrections for bleaching (http://www.embl-heidelberg.de/eamnet/html/body_bleach_correction.html) and cell movements (http://bigwww.epfl.ch/thevenaz/stackreg). An initial control image was taken immediately before damage induction. The average fluorescence signals were corrected for the background levels and normalized to the mean intensity of the same nuclear region before irradiation. Foci of UV lesions or DNA-repair factors in paraformaldehyde-fixed cells were quantified by using the LAS AF lite v1.9 software (Leica, Wetzlar, Germany).

### *Protein dynamics in living cells*

To carry out fluorescence recovery after photobleaching (FRAP) analyses, CHO cells were grown on glass coverslips and transfected as described earlier. Cells with low expressions of GFP fusions were subjected to high-time resolution FRAP by using a Leica TCS SP5 confocal microscope equipped with an $Ar^+$ laser (488 nm) and a ×63 oil-immersion lens (numeric aperture of 1.4). The assays were performed in a controlled environment at 37°C and with a $CO_2$ supply of 5%. A region of interest (ROI) of 4 $mm^2$ was photobleached for 2.3 s at 80% laser intensity. Fluorescence recovery within the ROI was monitored 200 times by using 115-ms intervals followed by 30 frames at 250 ms and 20 frames at 500 ms. Simultaneously, a reference ROI of the same size was measured for each time point to correct for overall bleaching. Finally, the data were normalized to the prebleach intensity.

FRAP on local damage (FRAP-LD) was applied to test the stability of XPC interactions with damaged sites. In CHO cells transfected with GFP fusion constructs, ROIs corresponding to foci of XPC accumulation were defined 15–30 min after UV-C irradiation (254 nm, 150 $J/m^2$) through polycarbonate filters. These ROIs were photobleached until the fluorescence reached a level equivalent to that of the nuclei around the foci. Fluorescence recovery within each ROI was monitored through a ×40 oil-immersion objective lens with a numeric aperture of 1.4. The measurements were conducted 10 times by using 700-ms intervals followed by 10 frames of 5 s and six frames of 20 s. Simultaneously, a reference ROI of the same size was measured for each time point to correct for overall bleaching. The values were used to calculate ratios between the damaged areas in the foci and the corresponding intensity before bleaching. In the data display, the first fluorescence measurement after photobleaching is set to 0 (1).

### *Host-cell reactivation assay*

pGL3 and phRL-TK vectors expressing firefly (*Photinus*) and *Renilla* luciferase were purchased from Promega (Dübendorf, Switzerland). The pGL3 DNA was UV-irradiated (257 nm, 1,000 $J/m^2$) in 10 m*M* Tris-HCl (pH 8) and 1 m*M* EDTA. Human XP–C fibroblasts, grown to a confluence of 80% in six-well plates, were transfected with 0.5 $\mu$g XPC-pEGFP expression vector, 0.45 $\mu$g irradiated pGL3 DNA, and 0.05 $\mu$g phRL-TK. After a 4-h incubation, the transfection reagent was replaced by complete medium. The cells were lysed after a further 18-h period by using 0.5 ml Passive Lysis Buffer (Promega), following the manufacturer's instructions. *Photinus* and *Renilla* luciferase activity was determined in a Dynex microtiter plate luminometer by using the Dual-Luciferase Assay System (Promega). Mean values were calculated from the ratios between *Photinus* and *Renilla* luciferase activity.

### *Statistical analysis*

Results are expressed as mean ± SD or mean ± SEM of at least three independent experiments in each group. The statistical analysis was performed with InStat 3.0 Software for Macintosh (GraphPad Software) by using the Student *t* test for comparisons. A value of $p < 0.05$ was considered statistically significant.

## Results

### *DNA-binding activity* in vitro

Human XPC was overexpressed in *Sf*9 insect cells, as a fusion with maltose-binding protein (MBP), and cell lysates containing quantitatively similar levels of wild-type and mutant MBP-XPC were identified with immunoblotting (Fig. 2A). The DNA-binding activity was determined in pull-down assays by incubation with radiolabeled substrates displaying the same length but different conformations (*i.e.*, homoduplex fragments of 135 base pairs, single-stranded 135-mer oligonucleotides, or junction molecules consisting of a duplex region of 71 base pairs with single-stranded overhangs of 64 nucleotides). Dose–response experiments were conducted with increasing amounts of cell lysate (Fig. 2B) to determine a nonsaturating concentration of wild-type XPC protein (1.7 n*M*) for comparisons with site-directed mutants containing single alanine substitutions.

This *in vitro* DNA-binding assay demonstrates that the tested amino acids are indeed critical for the interaction of XPC protein with DNA. With all substrate conformations, the three mutations, N754A, F756A, and F797A, confer a more severe DNA-binding defect than the F799A substitution (Fig. 2C). However, all four mutants are essentially unable to interact with the single-stranded oligonucleotides. A surprising observation is that the four site-directed mutants also display a reduced binding to homoduplex DNA (Fig. 2C). Thus, residues N754, F756, F797, and F799, selected in view of their affinity for the single-stranded configuration of extrahelical nucleotides, also contribute in a substantial manner to the binding of XPC protein to undamaged DNA in its native double helical form.

### *DNA-damage recognition in tracks of UV lesions*

The ability to recognize DNA damage in living cells was tested by monitoring the accumulation of green-fluorescent protein (GFP) constructs along high-resolution tracks of UV lesions. The XPC subunit is normally assisted in the recognition of UV photoproducts by an accessory factor known as

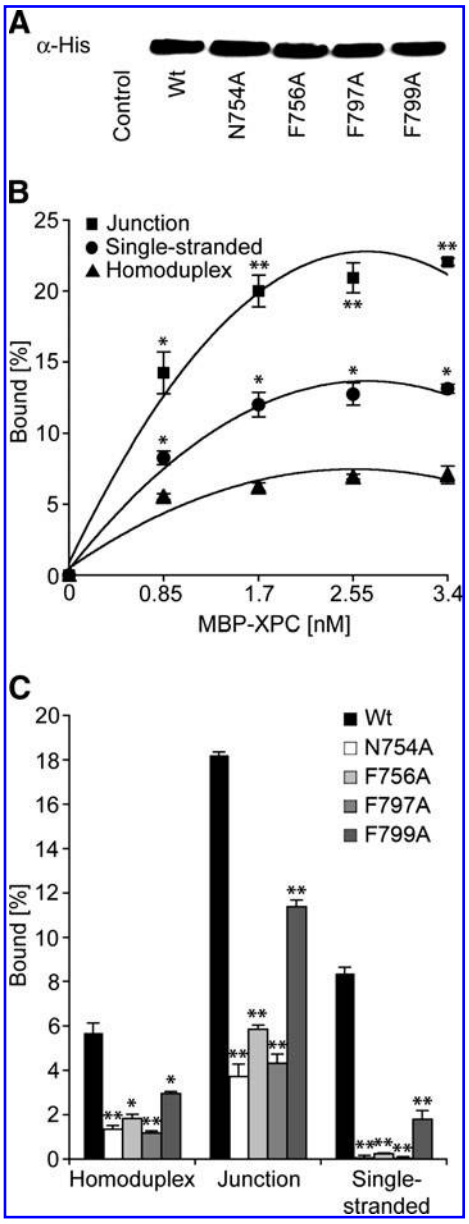


**FIG. 2. DNA-binding defect of XPC mutants *in vitro*. (A)** Immunoblot of *Sf*9 cell lysates (50 $\mu$g of total protein) demonstrating similar amounts of MBP-XPC fusions. Control, lysate from uninfected cells; Wt, wild-type. **(B)** Binding of XPC protein to single-stranded, double-stranded, or junction DNA. The indicated concentrations of MBP-XPC in cell lysate were incubated with $^{32}$P-labeled 135-mer substrates (2 n*M*). The DNA captured by XPC protein was separated from the free oligonucleotides and quantified in a scintillation counter. The bound fraction is reported as the percentage of total input DNA. Asterisks, statistically significant differences between the binding to junction and single-stranded oligonucleotides and the homoduplex control (mean ± SD; $*p < 0.001$, $**p < 0.0001$; $N = 3$). **(C)** Comparison of DNA-binding activity of wild-type and mutant XPC protein (1.7 n*M*) in the presence of the indicated substrates. *Asterisks*, statistically significant differences of the mutants from wild-type protein (mean ± SD; $*p < 0.05$; $**p < 0.0001$; $N = 3$).

UV-damaged DNA-binding (UV-DDB) protein (16). To avoid this stimulatory effect of UV-DDB and, hence, to determine the intrinsic function of XPC protein in detecting DNA damage, nuclear-relocation experiments were performed in Chinese hamster ovary (CHO) cells, which are devoid of UV-DDB activity because they fail to express its DNA-binding subunit DDB2 (40).

After transfection with appropriate vectors, individual CHO cells expressing low levels of XPC-GFP fusions, in the range of endogenous XPC in human fibroblasts (8), were identified by measuring the overall nuclear fluorescence. Next, 10-$\mu$m tracks of UV lesions were produced by application of a multiphoton laser that achieves high spatial resolution with minimal collateral damage (29, 41). The subsequent real-time redistribution of XPC-GFP was assessed by recording the local increase in fluorescence intensity along each laser track (Fig. 3A). Wild-type XPC protein responded to local irradiation by reallocating to the damaged areas with an accumulation half-life of ~15 s (Fig. 3B). Already after ~50 s, a plateau level was reached, reflecting a steady-state condition with constant turnover. In contrast, the N754A, F756A, F797A, and F799A single mutants relocated to the UV lesion

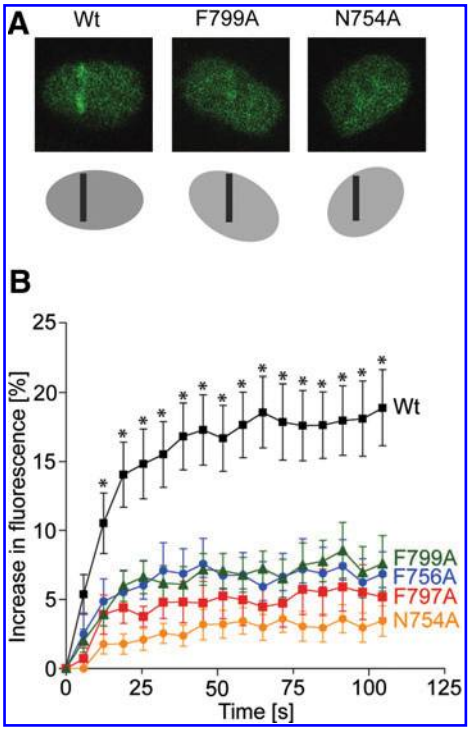


**FIG. 3. Real-time accumulation in tracks of UV lesions. (A)** Representative images illustrating the differential accumulation of wild-type and mutant XPC protein at lesion sites. CHO cells expressing low levels of XPC-GFP were laser treated to generate 10-$\mu$m tracks of UV lesions. *Black bars*, position of the 10-$\mu$m irradiation track. **(B)** Real-time kinetics of DNA-damage recognition. The accumulation of XPC-GFP (wild-type or mutants) at different time points is plotted as a percentage of the average fluorescence before irradiation. *Asterisks*, statistically significant differences of wild-type XPC compared with the mutants (mean ± SEM; $*p < 0.05$; $N = 10$). (To see this illustration in color the reader is referred to the web version of this article at www.liebertonline.com/ars).

tracks with prolonged half-lives of accumulation and markedly reduced plateau levels (Fig. 3B). These results demonstrate that all four tested amino acid side chains are required for the formation of a DNA-damage–recognition intermediate in the chromatin of living cells. The most severe reduction of local accumulation is caused by the N754A change.

### *DNA-damage recognition in UV foci*

In addition to UV photoproducts, irradiation by the multiphoton laser causes oxidative damage and DNA strand breaks. The nuclear-relocation experiments were, therefore, confirmed by generating UV-C foci containing essentially only cyclobutane pyrimidine dimers and (6-4) photoproducts (8, 14, 26). For that purpose, CHO cells transfected with XPC-GFP constructs were UV irradiated (254 nm wavelength) through the pores of polycarbonate filters, thereby localizing the DNA damage to small nuclear spots. After a 15-min recovery at 37°C, the cells were subjected to paraformaldehyde fixation to visualize the co-localization of (6-4) photoproducts and XPC-GFP fusions. As shown in Fig. 4, wild-type XPC protein generated bright green foci with reduced overall nuclear fluorescence, indicative of a strong accumulation in damaged sites with a concomitant depletion of the GFP fusion from undamaged regions. The XPC single mutants also relocated to the damaged foci but to a lower degree, generating weaker green fluorescence signals over the surrounding nuclear area. An exact quantitative comparison between the mutations is limited by the wide heterogeneity of size, shape, and photoproduct density of the foci, but, on the average, the four mutants reached a local fluorescence intensity above background that was only ~30% of that observed with the wild-type control ($N = 30$). These results support the notion that all tested amino acids (N754, F756, F797, and F799) are required for the formation of a DNA-damage–recognition intermediate in living cells.

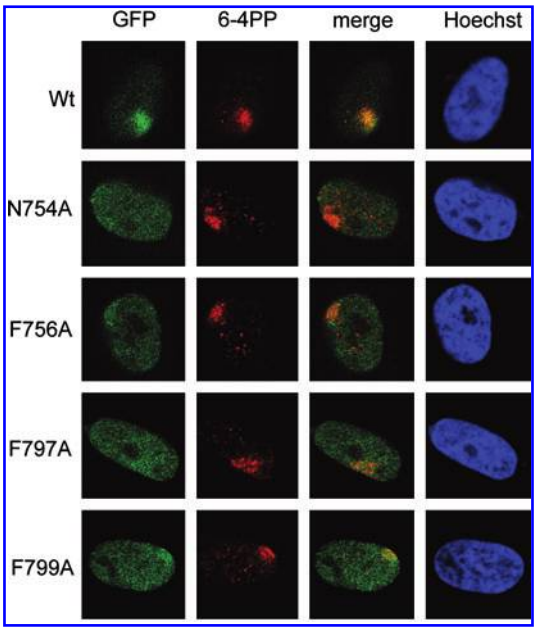


**FIG. 4. Acccumulation in foci of UV lesions.** Representative images illustrating that the site-directed mutants are defective in the reallocation to UV foci relative to the wild-type control. CHO cells were irradiated through the pores of polycarbonate filters and fixed 15 min after treatment to monitor the co-localization of the GFP fusion constructs (green) and (6-4) photoproducts (red). Hoechst, DNA staining visualizing the nuclei. (To see this illustration in color the reader is referred to the web version of this article at www.liebertonline.com/ars).

### *Overall nuclear dynamics of XPC protein*

The interaction of XPC protein with genomic DNA before and after UV irradiation was examined with fluorescence recovery after photobleaching (FRAP), which is a powerful real-time method to probe the nuclear mobility of repair proteins (1, 22). In cells containing low levels of each XPC-GFP fusion, a 4-$\mu m^2$ area of the nucleus was bleached with a laser (488 nm wavelength, not producing DNA damage) to eliminate the fluorescence signal. Subsequently, the gradual recovery of fluorescence within the bleached area, due to the rapid diffusion of free XPC-GFP molecules, is recorded over time. In non-irradiated CHO cells, when the DNA contains no UV lesions, the bleached spot ultimately reaches a fluorescence intensity equal to that detected before the photobleaching process (Fig. 5A). After UV irradiation (20 $J/m^2$), this fluorescence recovery is significantly delayed, indicating that the movements of XPC protein are restrained as a consequence of its binding to UV lesions. The UV dose of 150 $J/m^2$, used to saturate the XPC molecules with a high lesion density, further delays the recovery of fluorescence, reflecting an immobilization of the fusion proteins in response to DNA damage (22).

The FRAP analysis was used for a direct comparison of protein dynamics between wild-type XPC and the single mutants (N754A, F756A, F797A, F799A). In non-irradiated cells (*i.e.*, in the absence of UV lesions), the alanine substitution N754A and, to a lesser extent, the F797A and F799A mutations, retarded the fluorescence recovery (Fig. 5B). This unanticipated finding indicates that the DNA-binding defect of these mutants (see Fig. 2C) restricts their normal nuclear mobility in comparison to the wild-type control. When the cells were UV irradiated, the nuclear dynamics of the four tested mutants was not affected by their encounters with DNA lesions (Fig. 5C–F), lending further support to the conclusion that the loss of one of the tested XPC side chains is sufficient to prevent the formation of a stable recognition complex.

### *XPC protein dynamics in UV foci*

Among the tested mutants, F756A and F799A display the highest residual accumulation in the quantitative laser track assay of Fig. 3B. To compare the stability of the interactions that these mutants undergo with damaged genomic DNA, UV-induced foci containing the respective fusion proteins were analyzed with fluorescence recovery after photobleaching on local damage (FRAP-LD) (1). To that end, the green fluorescence of individual foci was photobleached until the signal reached the lower background level of the surrounding nuclear areas. The subsequent fluorescence recovery due to the exchange of bleached XPC molecules with nonbleached counterparts was again recorded over time, thus yielding distinct dissociation curves (Fig. 6). In particular, we

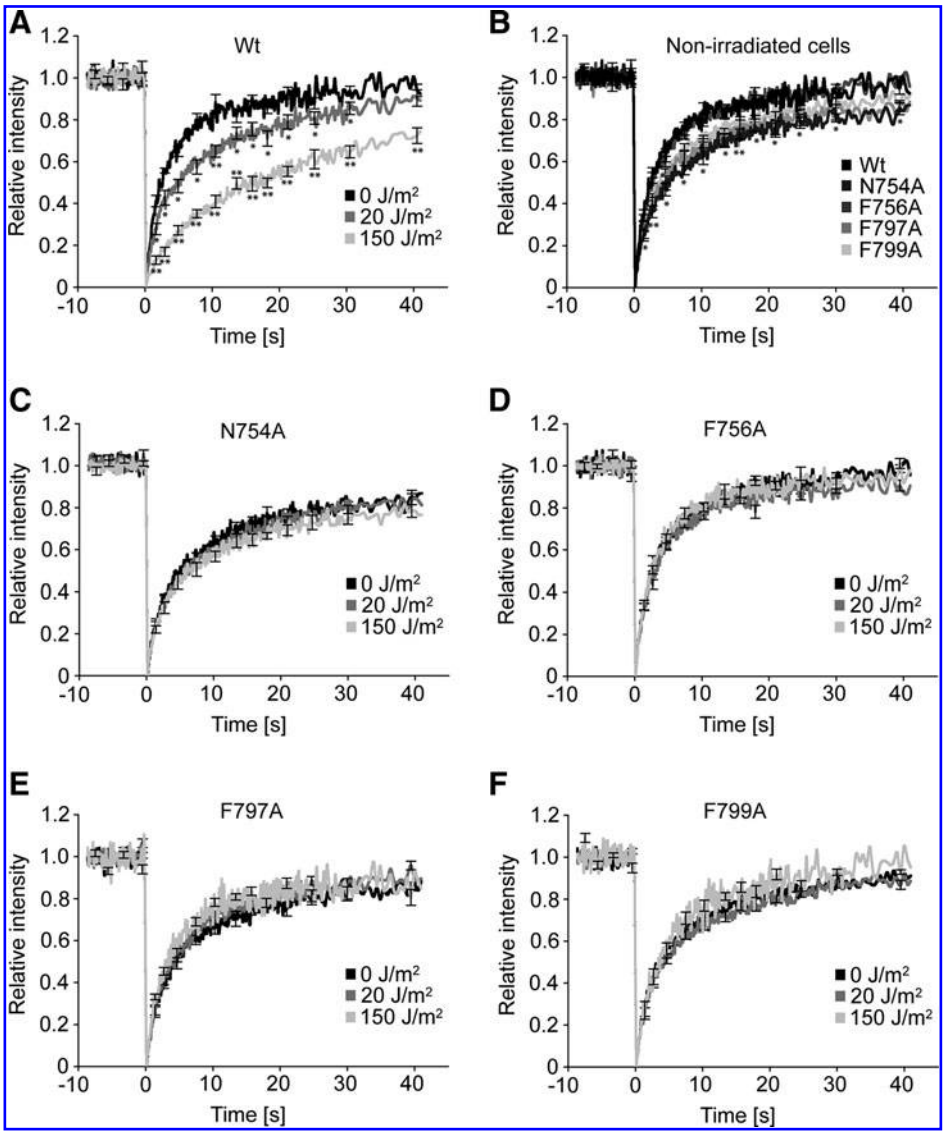


**FIG. 5. Analysis of protein dynamics in the nuclei of living cells**. In CHO cells expressing the indicated XPC-GFP constructs, a nuclear area of 4 $\mu m^2$ is bleached with a 488-nm wavelength laser. The subsequent fluorescence recovery depends on the diffusion rate and macromolecular interactions (8, 22). **(A)** Response of wild-type XPC protein to UV irradiation. Asterisks, statistically significant differences of UV-irradiated compared with nonirradiated cells (mean ± SEM; $*p < 0.05$; $**p < 0.0001$; $N = 12$). **(B)** Differential movements of wild-type and mutant XPC protein in nonirradiated cells. The order of protein mobility is as follows: Wt = F756A > F799A > F797A > N754A. *Asterisks*, statistically significant differences of N754A compared with the wild-type control (mean ± SEM; $*p < 0.05$; $**p < 0.0001$; $N = 10$). **(C–F)** The nuclear mobility of the indicated XPC mutants is not retarded by UV irradiation (n = 12, ± SEM).

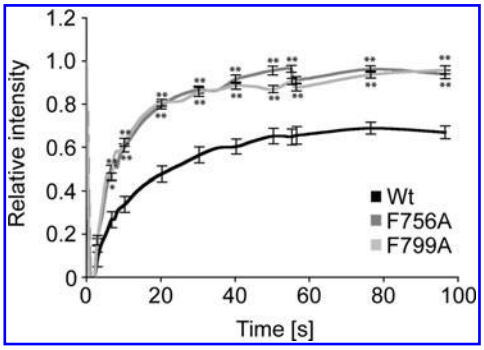


**FIG. 6. Dissociation from sites of UV damage in living cells.** The green signal representing XPC-GFP fusion proteins in the UV foci of CHO cells was bleached to reach the overall fluorescence intensity of the surrounding nuclear area. The differential recovery of fluorescence in the bleached spots indicates that only wild-type XPC forms stable recognition complexes. Asterisks, statistically significant differences of the mutants from wild-type control (mean ± SEM; $*p < 0.001$; $**p < 0.0001$; $N = 10$).

observed that the fluorescence of the F756A and F799A mutants reached the prebleach intensity after ~30 s, indicating that they readily dissociate from UV-irradiated sites. Instead, wild-type XPC protein forms a subset of stable complexes in the UV foci in a manner that the final plateau of fluorescence remains significantly below the prebleach signal (Fig. 6). Thus, this analysis of local protein dynamics confirms that, despite its more moderate contribution to DNA binding (see Fig. 2C), the side chain of F799 is nevertheless necessary for the anchoring of XPC protein onto damaged DNA.

### *XPC-dependent recruitment of TFIIH complexes*

Once bound to damaged DNA, XPC protein serves as a platform for the loading of transcription factor TFIIH onto the substrate (39, 48). Therefore, we next tested how the different mutations affect the ability of XPC protein to recruit TFIIH to lesion sites. For that purpose, XP-C fibroblasts lacking functional *XPC* were complemented by transfection with XPC-GFP fusion vectors. Foci of UV lesions were generated by irradiation through micropore filters and, after 30 min, the cells were processed by immunocytochemistry to stain the

TFIIH subunits p62 and p89 with a red-fluorescent dye. Finally, the UV-dependent colocalization of XPC protein and TFIIH was assessed by quantifying the green and red signals, respectively, in nuclear foci.

In the case of wild-type XPC, the accumulation of GFP fusion protein translates to the recruitment of p62 within the UV-irradiated areas. However, the redistribution of this TFIIH subunit is not observed in XP-C cells expressing the F799A mutant (Fig. 7A) or in XP-C cells transfected with the empty pEGFP vector (data not shown). To perform quantitative comparisons, the ratio of fluorescence over background was determined in each focus, whereby the green fluorescence stands for the accumulation of XPC protein, and the red fluorescence represents the p62 (Fig. 7B) or p89 subunits (Fig. 7C). This quantitative analysis revealed that the N754A and F756A mutants fully retain the ability to engage TFIIH. Instead, the F797A and F799A mutations result in a decreased recruitment of the TFIIH complex to lesion sites. This conclusion is supported by the observation that the F797A/F799A double mutant still accumulates in the UV foci of XP-C cells but, unlike the N754A/F756A double mutant, is unable to hand over the lesions to the downstream TFIIH machinery.

It should be pointed out that, in these experiments performed with human fibroblasts, the UV-dependent redistribution of the different mutants is slightly more effective than that in the comparable assay of Fig. 4 carried out with CHO cells. This difference is attributable to the fact that CHO cells lack DDB2, the DNA-binding subunit of UV-DDB, which in human cells stimulates the relocation of XPC protein to UV foci produced by the micropore filter method (47). Therefore, we performed additional control experiments to show that the overexpression of DDB2-GFP alone, in the absence of XPC protein, is not sufficient to recruit the p62 and p89 subunits (Fig. 7B and 7C). Thus, the differential transfer of UV lesions to the TFIIH complex represents a genuine property of the tested XPC mutants and reflects the contribution of the respective amino acid side chains to the conformational rearrangements necessary for the loading of this downstream factor onto damaged DNA.

### *GGR activity in human cells*

Finally, the repair proficiency of each mutant was tested by expressing XPC-GFP constructs in GGR-deficient XP-C fibroblasts (Fig. 8A). The degree of functional complementation was determined by a host-cell reactivation assay that has been developed to measure the cellular GGR activity (9) and that is performed by co-transfection with a dual luciferase system. The reporter plasmid, damaged by UV-C irradiation, carries a *Photinus* luciferase gene, whereas the undamaged control codes for the *Renilla* luciferase (28). After an 18-h incubation, the activity of *Photinus* luciferase, the expression of which depends on the repair of UV lesions, was measured in cell lysates and normalized against the accompanying *Renilla* counterpart. In XP-C fibroblasts transfected with the empty pEGFP vector, the luciferase expression is reduced to background levels consistent with the absence of GGR activity in this cell line (Fig. 8B). Compared with wild-type XPC, all tested single mutants display a repair defect leading to reduced expression of the luciferase reporter. The mildest response was associated with the F756A substitution, consistent with the observation that this mutant is only partially

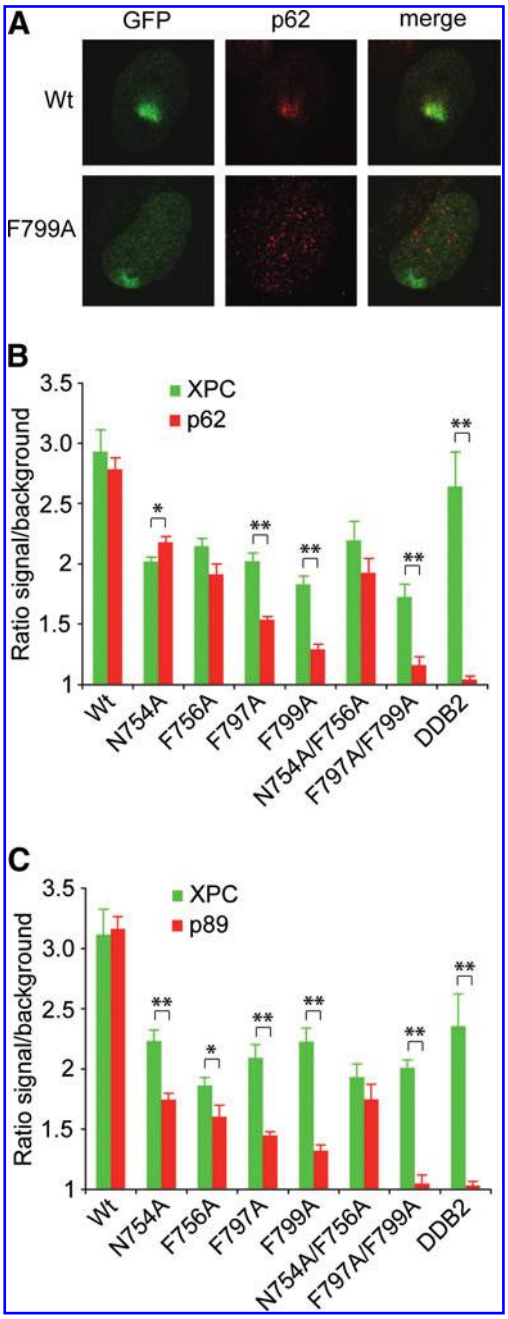


**FIG. 7. Recruitment of TFIIH. (A)** Representative images illustrating that wild-type XPC but not the F799A mutant is able to recruit the p62 subunit of TFIIH to UV foci. **(B, C)** Quantitative assessments of green and red signals representing the accumulation of XPC-GFP and the indicated TFIIH subunits, respectively, in XP-C fibroblasts. Foci of DNA damage were generated by UV-C irradiation through micropore filters. The recruitment of p62 and p89 is determined by immunocytochemistry. *Asterisks*, statistically significant differences between the accumulation of p62 and p89, respectively, and the accumulation of XPC protein (mean ± SEM; $*p < 0.05$; $**p < 0.0001$; $N = 30$). (To see this illustration in color the reader is referred to the web version of this article at www.liebertonline.com/ars).

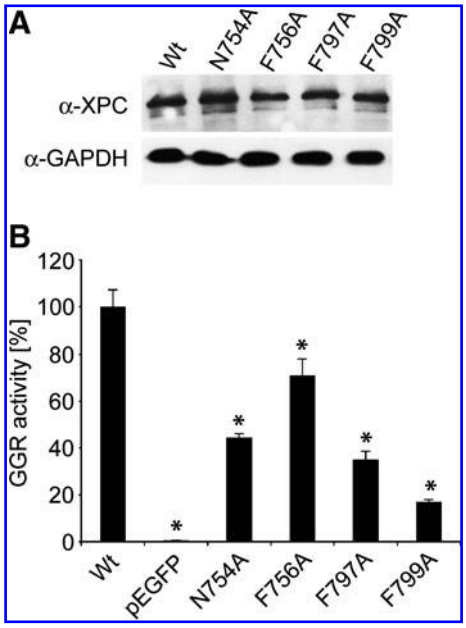


**FIG. 8. GGR activity. (A)** Representative immunoblot to compare the expression of XPC-GFP fusion proteins in XP-C fibroblasts. **(B)** The repair of UV lesions was determined by means of a host-cell reactivation assay. *Asterisks*, statistically significant differences from the wild-type protein control (mean ± SD; $*p < 0.0001$; $N = 9$). Reactivation of the luciferase reporter is plotted as the percentage of controls determined by transfecting cells with the vector coding for wild-type XPC-GFP; pEGFP, background luciferase expression in cells transfected with the empty vector.

impaired in its ability to relocate to tracks of UV lesions but is fully proficient in the subsequent TFIIH recruitment (see Figs. 3B and 7). In contrast, the most severe GGR defect was imposed by the F799A mutation, which is in line with the finding that this amino acid is very critical for the recruitment of TFIIH to lesion sites.

## Discussion

The present analysis of human XPC protein, based on site-directed mutagenesis, was instigated by the intriguing configuration of DNA found in crystal complexes of the yeast Rad4 homologue with a model substrate (30). In this previous structural study, Rad4 protein binds to damaged duplexes by interacting with a double-stranded to single-stranded DNA transition around the lesion site, whereby two neighboring nucleotides in the undamaged strand are completely displaced out of the double helix. Conserved amino acids (N754, F756, F797, and F799) predicted to make close contacts with these flipped-out nucleotides have been identified in the human XPC sequence and challenged by alanine substitutions (Fig. 1). The results of our study demonstrate that the four tested residues indeed play a key role in the formation of a recognition intermediate that transfers the DNA lesions to downstream GGR factors.

The most crucial outcome of this study is that the examined side groups drive a sequence of distinguishable nucleoprotein transitions starting from the default search mode, by which XPC protein finds DNA damage in the genome, to an initial (unstable) encounter complex at lesion sites and, finally, the installation of an ultimate (stable) recruitment platform. The variable effects of alanine substitutions at different XPC positions imply that the respective amino acid residues exert diverging functions during the aforementioned transitions. In the *in vitro* assay, the interaction with DNA is more sensitive to N754A, F756A, and F797A substitutions than to the corresponding change at position F799. The most prominent difference between the N754A, F756A, and F797A mutations and the F799A substitution was observed with the junction DNA molecule (Fig. 2C) used as a model substrate to probe the affinity of XPC protein for unpaired bases in a duplex context. The common binding partner of residues N754, F756, and F797 is the flipped-out base on the 3′ side of the undamaged strand (Fig. 1B), suggesting that these three side chains of XPC protein cooperate to sense damage-induced base displacements opposite to lesion sites. Conversely, the F799A mutation conveys a more severe reduction in the binding to single-stranded DNA relative to junction molecules, indicating that this residue is nevertheless important to stabilize XPC protein onto the displaced undamaged strand. This view is supported by FRAP-LD analyses, indicating that the F799A mutant is unable to anchor itself onto UV-irradiated DNA in living cells (Fig. 6).

A separation of function between the tested amino acid residues was also evident when we monitored the subsequent TFIIH recruitment. Both the N754A and F756A mutations diminish the relocation to UV foci, but the fraction of these XPC mutants that did accumulate at lesion sites was as effective as the wild-type control in engaging TFIIH into the nascent GGR complex. Instead, the F797A and, particularly, the F799A mutation interfered with TFIIH recruitment (Fig. 7). The common binding partner of F797 and F799 is the flipped-out residue on the 5′ side (Fig. 1), thus indicating that the extrusion of this additional nucleotide is essential for the transfer of DNA lesions from XPC protein to TFIIH. These findings are consistent with a previous truncation study, indicating that the detection of damaged sites is mediated mainly by a dynamic interface of XPC protein that includes amino acids 607–766, whereas an adjacent protein segment (amino acids 767–833) is required for the following stabilization of a GGR-initiating complex on the target substrate (8).

Surprisingly, our mutagenesis analysis revealed that the side chains of XPC protein that interact with the flipped-out nucleotides in the ultimate recognition complex also contribute to the default binding to native double-stranded DNA (Fig. 2C). This finding is at first sight counterintuitive because it may have been expected that an amino acid substitution that reduces the affinity for the native duplex, and hence suppresses the interaction with genomic DNA, would cause an increased nuclear mobility in FRAP experiments. However, when this prediction was tested in undamaged living cells, we found that the N754A change actually limits the movements of XPC protein (Fig. 5B). Although less pronounced, a diminished nuclear mobility compared with wild-type was also found for the F797A and F799A mutants. A likely scenario that accommodates this surprising observation is that XPC protein searches for DNA lesions by a facilitated diffusion procedure, whereby protein movements within living cells are guided by interactions with DNA filaments. Facilitated protein diffusion may occur by a "sliding" mode (*i.e.*, by movements along linear molecules) or by a "hopping"

mode that involves continuous association–dissociation cycles from one site to another on DNA. In either case, by reducing the dimensionality of the search process, facilitated diffusion is thought to enhance the efficiency of target-site location by several orders of magnitude (5, 49). Support for the involvement of N754 in a facilitated search process comes from the observation that the low mobility conferred by the exchange of this residue with alanine (Fig. 5B) correlates with the weakest accumulation of all mutants in UV lesion tracks (Fig. 3B).

In summary, this study describes how four critical amino acid side chains of human XPC protein interact with multiple DNA conformations to drive the genome-wide search process, the formation of a dynamic (unstable) encounter complex, and the installment of a stable recognition intermediate that promotes TFIIH recruitment. The GGR proficiency of the tested XPC mutants reflects the cumulative effect of the respective amino acid substitutions on these distinguishable but interrelated activities of XPC protein. Further studies will be devoted to analyze the contribution of UV-DDB and chromatin-remodeling complexes in this genome-wide lesion-recognition mechanism.

## Acknowledgments

We thank A. Lenisa, M. Träxler, and D. Hermann for excellent technical assistance, G. Marra (University of Zürich) for the gift of CHO cells, and S. Linn (University of California, Berkeley) for the DDB2-GFP expression vector.

## Author Disclosure Statement

No competing financial interests exist.

## References

1. Alekseev S, Luijsterburg, MS, Pines A, Geyerts B, Mari PO, Giglia-Mari G, Lans H, Houtsmuller AB, Mullenders LH, Hoeijmakers JH, and Vermeulen W. Cellular concentrations of DDB2 regulate dynamic binding of DDB1 at UV-induced DNA damage. *Mol Cell Biol* 28:7402–7413, 2008.
2. Andressoo JO, Hoeijmakers JH, and Mitchell JR. Nucleotide excision repair disorders and the balance between cancer and aging. *Cell Cycle* 5: 2886–2888, 2006.
3. Araujo SJ, Tirode F, Coin F, Pospiech H, Syväoja JE, Stucki M, Hübscher U, Egly JM, and Wood RD. Nucleotide excision repair of DNA with recombinant human proteins: definition of the minimal set of factors, active forms of TFIIH, and modulation by CAK. *Genes Dev* 14: 349–359, 2000.
4. Batty D, Rapic'-Otrin V, Levine AS, and Wood RD. Stable binding of human XPC complex to irradiated DNA confers strong discrimination for damaged sites. *J Mol Biol* 300: 275–290, 2000.
5. Berg OG, Winter RB, and van Hippel PH. Diffusion-driven mechanisms of protein translocation on nucleic acids, 1: models and theory. *Biochemistry* 20: 6929–6948, 1981.
6. Brooks PJ. The case for 8,5′-cyclopurine-2′-deoxynucleosides as endogenous DNA lesions that cause neurodegeneration in xeroderma pigmentosum. *Neuroscience* 145: 1407–1417, 2007.
7. Buterin T, Meyer C, Giese B, and Naegeli H. DNA quality control by conformational readout on the undamaged strand of the double helix. *Chem Biol* 12: 913–922, 2005.
8. Camenisch U, Träutlein D, Clement FC, Fei J, Leitenstorfer A, Ferrando-May E, and Naegeli H. Two-stage dynamic DNA quality check by xeroderma pigmentosum group C protein. *EMBO J* 28: 2387–2399, 2009.
9. Carreau M, Quilliet X, Eveno E, Salvetti A, Danos O, Heard JM, Mezzina M, and Sarasin A. Functional retroviral vector for gene therapy of xeroderma pigmentosum group D patients. *Hum Gene Ther* 6: 1307–1315, 1995.
10. Chavanne F, Broughton BC, Pietra D, Nardo T, Browitt A, Lehmann AR, and Stefanini M. Mutations in the XPC gene in families with xeroderma pigmentosum and consequences at the cell, protein and transcription level. *Cancer Res* 60: 1974–1982, 2000.
11. Cleaver JE. Cancer in xeroderma pigmentosum and related disorders of DNA repair. *Nat Rev Cancer* 5: 564–573, 2005.
12. Cleaver JE, Thompson LH, Richardson AS, and States JC. A summary of mutations in the UV-sensitive disorders: xeroderma pigmentosum, Cockayne syndrome, and trichothiodystrophy. *Hum Mutat* 14: 9–22, 1999.
13. Cosman M, Fiala R, Hingerty BE, Laryea A, Lee H, Amin S, Geacintov NE, Broyde S, and Patel D. Solution conformation of the (+)-trans-anti[BPh]dA adduct opposite dT in a DNA duplex: intercalation of the covalently attached benzo[c]phenanthrene to the 5′-side of the adduct site without disruption of the modified base pair. *Biochemistry* 32: 12488–12497, 1993.
14. Dinant C, de Jager M, Essers J, van Cappellen WA, Kanaar R, Houtsmuller AB, and Vermeulen W. Activation of multiple DNA repair pathways by subnuclear damage induction methods. *J Cell Sci* 120: 2731–2740, 2007.
15. Evans E, Moggs JG, Hwang JR, Egly JM, and Wood RD. Mechanism of open complex and dual incision formation by human nucleotide excision repair factors. *EMBO J* 16: 6559–6573, 1997.
16. Fitch ME, Nakajima S, Yasui A, and Ford JM. In vivo recruitment of XPC to UV-induced cyclobutane pyrimidine dimers by the DDB2 gene product. *J Biol Chem* 278: 46906–46910, 2003.
17. Friedberg EC. How nucleotide excision repair protects against cancer. *Nat Rev Cancer* 1: 22–33, 2001.
18. Friedberg EC, Walker GC, Siede W, Wood RD, Schultz RA, and Ellenberger T. *DNA Repair and Mutagenesis*. Washington, DC: ASM Press, 2006, p. 698.
19. Gillet LC and Schärer OD. Molecular mechanisms of mammalian global genome nucleotide excision repair. *Chem Rev* 106: 253–276, 2006.
20. Hanawalt PC and Spivak G. Transcription-coupled DNA repair: two decades of progress and surprises. *Nat Rev Mol Cell Biol* 9: 958–970, 2008.
21. Hoeijmakers JH. DNA damage, aging, and cancer. *N Engl J Med* 361: 1475–1485, 2009.
22. Hoogstraten D, Bergink S, Verbiest VH, Luijsterburg MS, Geverts B, Raams A, Dinant C, Hoeijmakers JH, Vermeulen W, and Houtsmuller AB. Versatile DNA damage detection by the global genome nucleotide excision repair protein XPC. *J Cell Sci* 121: 2850–2859, 2008.
23. Huang JC, Svoboda DL, Reardon JT, and Sancar A. Human nucleotide excision nuclease removes thymine dimers from DNA by incising the 22$^{nd}$ phosphodiester bond 5′ and the 6$^{th}$ phosphodiester bond 3′ to the photodimer. *Proc Natl Acad Sci U S A* 89: 3664–3668, 1992.
24. Kim JK, Soni SD, Arakali AV, Wallace JC, and Alderfer JL. Solution structure of a nucleic acid photoproduct of deoxyfluorouridylyl-(3′-5′)-thymidine monophosphate (d-FpT)

determined by NMR and restrained molecular dynamics: structural comparison of two sequence isomer photoadducts (d-U5p5T and d-T5p5U). *Nucleic Acids Res* 23: 1810–1815, 1995.
25. Kim JK and Choi BS. The solution structure of DNA duplex-decamer containing the (6-4) photoproduct of thymidylyl (3′→5′)thymidine by NMR and relaxation matrix refinement. *Eur J Biochem* 228: 849–854, 1995.
26. Lan L, Nakajima S, Oohata Y, Takao M, Okano S, Masutani M, Wilson SH, and Yasui A. In situ analysis of repair processes for oxidative DNA damage in mammalian cells. *Proc Natl Acad Sci U S A* 101: 13738–13743, 2004.
27. Lehmann AR. DNA repair-deficient diseases, xeroderma pigmentosum, Cockayne syndrome and trichothiodystrophy. *Biochimie* 85: 1101–1111, 2003.
28. Maillard O, Solyom S, and Naegeli H. An aromatic sensor with aversion to damaged strands confers versatility to DNA repair. *PLoS Biol* 5: e79, 2007.
29. Meldrum RA, Botchway SW, Wharton CW, and Hirst GJ. Nanoscale spatial induction of ultraviolet photoproducts in cellular DNA by three-photon near-infrared absorption. *EMBO Rep* 4: 1144–1149, 2003.
30. Min JH and Pavletich NP. Recognition of DNA damage by the Rad4 nucleotide excision repair protein. *Nature* 449: 570–575, 2007.
31. Ng JM, Vermeulen W, van der Horst GT, Bergink S, Sugasawa K, Vrieling H, and Hoeijmakers JH. A novel regulation mechanism of DNA repair by damage-induced and RAD23-dependent stabilization of xeroderma pigmentosum group C protein. *Genes Dev* 17: 1630–1645, 2003.
32. Nishi R, Okuda Y, Watanabe E, Mori T, Iwai S, Masutani C, Sugasawa K, and Hanaoka F. Centrin 2 stimulates nucleotide excision repair by interacting with xeroderma pigmentosum group C protein. *Mol Cell Biol* 25: 5664–5674, 2005.
33. O'Donovan A, Davies AA, Moggs JG, West SC, and Wood RD. XPG endonuclease makes the 3′ incision in human DNA nucleotide excision repair. *Nature* 371: 432–435, 1994.
34. O'Handley SF, Sanford DG, Xu R, Lester CC, Hingerty BE, Broyde S, and Krugh TR. Structural characterization of an *N*-acetyl-2-aminofluorene (AAF) modified DNA oligomer by NMR, energy minimization, and molecular dynamics. *Biochemistry* 32: 2481–2497, 1993.
35. Sancar A. DNA excision repair. *Annu Rev Biochem* 65: 43–81, 1996.
36. Sijbers AM, de Laat WL, Ariza RR, Biggerstaff M, Wei YF, Moggs JG, Carter KC, Shell BK, Evans E, de Jong MC, Rademakers S, de Rooij J, Jaspers NG, Hoeijmakers JH, and Wood RD. Xeroderma pigmentosum group F caused by a defect in a structure-specific DNA repair endonuclease. *Cell* 86: 811–822, 1996.
37. Staresincic L, Fagbemi FA, Enzlin JH, Gourdin AM, Wijgers N, Dunand-Sauthier I, Giglia-Mari G, Clarkson SG, Vermeulen W, and Schärer OD. Coordination of dual incision and repair synthesis in human nucleotide excision repair. *EMBO J* 28: 1111–1120, 2009.
38. Sugasawa K. Regulation of damage recognition in mammalian global genome nucleotide excision repair. *Mutat Res* 685: 29–37, 2010.
39. Sugasawa K, Ng JM, Masutani C, Iwai S, van der Spek PJ, Eker AP, Hanaoka F, Bootsma D, and Hoeijmakers JH. Xeroderma pigmentosum group C protein complex is the initiator of global genome nucleotide excision repair. *Mol Cell* 2: 223–232, 1998.
40. Tang JY, Hwang BJ, Ford JM, Hanawalt PC, and Chu G. Xeroderma pigmentosum p48 gene enhances global genomic repair and suppresses UV-induced mutagenesis. *Mol Cell* 5: 737–744, 2000.
41. Träutlein D, Adler F, Moutzouris K, Jeromin A, Leitenstorfer A, and Ferrando-May E. Highly versatile confocal microscopy system based on a tunable femtosecond Er:fiber source. *J Biophoton* 1: 53–61, 2008.
42. Trego KS and Turchi JJ. Pre-steady-state binding of damaged DNA by XPC-hHR23B reveals a kinetic mechanism for damage discrimination. *Biochemistry* 45: 1961–1969, 2006.
43. Uchida A, Sugasawa K, Masutani C, Dohmae N, Araki M, Yokoi M, Ohkuma Y, and Hanaoka F. The C-terminal domain of the XPC protein plays a crucial role in nucleotide excision repair through interactions with transcription factor IIH. *DNA Rep* 1: 449–461, 2002.
44. Volker M, Mone MJ, Karmakar P, van Hoffen A, Schul W, Vermeulen W, Hoeijmakers JH, van Driel R, van Zeeland AA, and Mullenders LH. Sequential assembly of the nucleotide excision repair factors in vivo. *Mol Cell* 8: 213–224, 2001.
45. Wakasugi M and Sancar A. Assembly, subunit composition, and footprint of human DNA repair excision nuclease. *Proc Natl Acad Sci U S A* 95: 6669–6674, 1998.
46. Wood RD. DNA repair in eukaryotes. *Annu Rev Biochem* 65: 135–167, 1996.
47. Yasuda G, Nishi R, Watanabe E, Mori T, Iwai S, Orioli D, Stefanini M, Hanaoka F, and Sugasawa K. In vivo destabilization and functional defects of the xeroderma pigmentosum C protein caused by a pathogenic missense mutation. *Mol Cell Biol* 27: 6606–6614, 2007.
48. Yokoi M, Masutani C, Maekawa T, Sugasawa K, Ohkuma Y, and Hanaoka F. The xeroderma pigmentosum group C protein complex XPC-HR23B plays an important role in the recruitment of transcription factor IIH to damaged DNA. *J Biol Chem* 275: 9870–9875, 2000.
49. Zharkov D and Grollmann AP. The DNA trackwalkers: principles of lesion search and recognition by DNA glycosylases. *Mutat Res* 577: 24–54, 2005.

Address correspondence to:
*Prof. Hanspeter Naegeli*
*University of Zürich-Vetsuisse*
*Institute of Pharmacology and Toxicology*
*Winterthurerstrasse 260*
*CH-8057 Zürich*
*Switzerland*

*E-mail:* naegelih@vetpharm.uzh.ch

Date of first submission to ARS Central, June 17, 2010; date of acceptance, July 18, 2010.

**Abbreviations Used**

CHO = Chinese hamster ovary
DMEM = Dulbecco's modified Eagle's medium
EGFP = enhanced green-fluorescent protein
FCS = fetal calf serum
FRAP = fluorescence recovery after photobleaching
FRAP-LD = FRAP on local damage
GFP = green-fluorescent protein
GGR = global-genome repair
MBP = maltose-binding protein
PBS = phosphate-buffered saline
RPA = replication protein A
SD = standard deviation
SEM = standard error of the mean
TFIIH = transcription factor IIH
UV = ultraviolet
UV-DDB = UV-damaged DNA-binding
XP = xeroderma pigmentosum

**This article has been cited by:**

1. Tracy M. Neher , John J. Turchi . 2011. Current Advances in DNA Repair: Regulation of Enzymes and Pathways Involved in Maintaining Genomic StabilityCurrent Advances in DNA Repair: Regulation of Enzymes and Pathways Involved in Maintaining Genomic Stability. *Antioxidants & Redox Signaling* **14**:12, 2461-2464. [Abstract] [Full Text] [PDF] [PDF Plus]